A Computationally-Efficient Inverse Approach to Probabilistic Strain-Based Damage Diagnosis

James E. Warner[1], Jacob D. Hochhalter[1], William P. Leser[1], Patrick E. Leser[1], and John A. Newman[1]

[1] *NASA Langley Research Center, Hampton, VA, 23666, USA*
james.e.warner@nasa.gov

ABSTRACT

This work presents a computationally-efficient inverse approach to probabilistic damage diagnosis. Given strain data at a limited number of measurement locations, Bayesian inference and Markov Chain Monte Carlo (MCMC) sampling are used to estimate probability distributions of the unknown location, size, and orientation of damage. Substantial computational speedup is obtained by replacing a three-dimensional finite element (FE) model with an efficient surrogate model. The approach is experimentally validated on cracked test specimens where full field strains are determined using digital image correlation (DIC). Access to full field DIC data allows for testing of different hypothetical sensor arrangements, facilitating the study of strain-based diagnosis effectiveness as the distance between damage and measurement locations increases. The ability of the framework to effectively perform both probabilistic damage localization and characterization in cracked plates is demonstrated and the impact of measurement location on uncertainty in the predictions is shown. Furthermore, the analysis time to produce these predictions is orders of magnitude less than a baseline Bayesian approach with the FE method by utilizing surrogate modeling and effective numerical sampling approaches.

1. INTRODUCTION

Structural health monitoring (SHM) is the driving technology behind the transition from time-based to condition-based maintenance. Motivated by both safety and economic drivers, this paradigm shift from *offline* inspection to *online* (*i.e.*, while operating) monitoring is critically important to industries including manufacturing, aerospace, and defense that seek to detect damage in structural and mechanical systems at the earliest possible time. While SHM is in the process of making the transition into the application domain, the evolution of the technology to enable damage prognosis to forecast residual life has very few deployed applications (Farrar & Worden, 2013). As damage prognosis is inherently probabilistic in nature and presumes a properly characterized initial damage state, its practical use is predicated on not just the detection and localization of damage from SHM, but on a thorough assessment of the extent of the damage along with rigorous uncertainty quantification (UQ).

In order to deliver a more comprehensive online health management system for practical use, a SHM system should possess several key characteristics to enable integration with damage prognosis. Since an explicit quantification of damage is required for prognosis, model-based (inverse problem) SHM is preferred to a data-based approach since the latter is generally limited to detection and localization in the absence of training data from damage states (Barthorpe, 2010). In this case, high-fidelity modeling (*e.g.*, finite element analysis) is needed to allow for arbitrary geometries and damage types to be considered (limited only by sensitivity of sensors to the damage indices). The damage diagnosis approach must also effectively incorporate UQ to facilitate probabilistic prognostics rather than providing only deterministic assessments. Finally, in order to make online application of the framework feasible, the algorithms deployed must also be computationally-efficient. Unfortunately, model-based SHM with high-fidelity modeling implies time-consuming simulations and UQ often requires tens of thousands of such analyses, so achieving such an all-encompassing SHM framework is extremely challenging.

Traditionally, damage detection techniques have largely

been deterministic in nature and have identified structural anomalies based on changes in measured mechanical response (*e.g.*, vibrations (Kim & Stubbs, 2002; Mal, Ricci, Banerjee, & Shih, 2005), ultrasonic wave characteristics (Wang & Yuan, 2007; Kehlenbach & Hanselka, 2003), and strains (Krishnamurthy & Gallegos, 2011; Hochhalter, Krishnamurthy, Aguilo, & Gallegos, 2016)). While deterministic approaches have been successfully used to accurately locate and sometimes quantify damage in a computationally-efficient manner, these methods neglect the impact of uncertainty that is ubiquitous in real SHM systems due to effects such as sensor noise and modeling assumptions.

More recently, there has been increased focus on uncertainty quantification for damage diagnosis using Bayesian inference in order to explicitly account for measurement and model uncertainties in practice. Several studies (Moore, Murphy, & Nichols, 2011; Nichols, Link, Murphy, & Olson, 2010; Huhtala & Bossuyt, 2011) have used noisy vibrations data to detect structural damage, while in one such study (Nichols, Moore, & Murphy, 2011), the emphasis was on the development of an efficient numerical sampling algorithm for exploring the resulting probability distribution. A Bayesian imaging method was developed in (Peng, Saxena, Goebel, Xiang, & Liu, 2014) to probabilistically estimate delamination location and size in composite laminates using Lamb wave measurements. The work of (Yan, 2012) used Bayesian inference and the extended finite element method to inversely estimate the probability distribution of crack location and size using strain data. Most recently, (Prudencio, Bauman, Faghihi, Ravi-Chandar, & Oden, 2015) used displacement data to estimate the parameters of a continuum mechanics model within a Bayesian framework and used Kalman filters to update and evolve the system state in time.

Compared to deterministic methods, Bayesian approaches have the advantage of quantifying uncertainty in the estimates provided, but also incur a substantial computational penalty. Here, the computational expense results from the numerical sampling algorithms, *e.g.*, Markov Chain Monte Carlo (MCMC) (Gamerman & Lopes, 2006), which can exhibit slow convergence and involve the evaluation of a potentially time-consuming computational model for each sample drawn. To alleviate this computational burden, advanced MCMC methods have been developed to reduce sampling time by improving sampling convergence (Haario, Laine, & Mira, 2006; Nichols et al., 2011) or through parallelization of the algorithms themselves (Vrugt et al., 2009; Neiswanger & Xing, 2013; Prudencio & Cheung, 2012). Another common approach is to replace the original physics-based model with a computationally-efficient surrogate model using probabilistic spectral methods (Marzouk, Najm, & Rahn, 2006) or machine learning algorithms (Meeds & Welling, 2014).

The development of Bayesian inference approaches in conjunction with advanced MCMC methods and surrogate modeling remains relatively limited for model-based SHM applications. However, machine learning trained using physics-based models has been explored for efficient diagnosis. The works in (Katsikeros & Labeas, 2009; Sbarufatti, Manes, & Giglio, 2013) have demonstrated the use of artificial neural networks (ANNs) to build the inverse-maps directly from measured strains to crack location and length for rapid damage diagnosis. Most notably, (Sbarufatti et al., 2013) provided a comprehensive experimental validation of the SHM framework in a simplified structure resembling a helicopter fuselage, demonstrating the ability to effectively perform anomaly detection as well as damage localization and quantification. The uncertainty quantification effort, however, was limited to confidence intervals based off the scatter in predictions from various ANNs.

Motivated by online, integrated SHM and damage prognosis, this study presents a computationally-efficient approach to probabilistic, strain-based damage diagnosis and the extension and experimental validation of the preliminary work done in (Warner & Hochhalter, 2016). Probability distributions for unknown damage are inferred with Bayesian inference. A surrogate model trained via three-dimensional (3D) finite element modeling and an efficient MCMC approach is used to provide substantial computational speedup. While the framework is applicable to arbitrary component geometries and damage parameterizations as well as different sensor types, it is demonstrated on the problem of crack characterization in thin plates using measured strains. Experimental validation is carried out using digital image correlation (DIC) (Peters & Ranson, 1982) strain data in two cracked lab specimens. Access to full field DIC data facilitates the study of the effectiveness of strain-based diagnosis as the distance between the locations of damage and strain measurements is varied.

The remainder of the paper is organized as follows. First, a complete formulation of the proposed damage diagnosis approach is provided in the following section, with individual subsections devoted to the Bayesian formulation, surrogate modeling, and the MCMC sampling method used. Next, experimental validation of the

method is provided. In this section, the experimental strain data obtained with digital image correlation, the development and performance of the surrogate models used, and results of the damage diagnosis method applied to both damage localization and characterization in two separate cracked lab specimens are presented. Finally, the findings of the study are summarized in the conclusion section.

2. FORMULATION

In this section, the proposed approach to probabilistic damage diagnosis using measured strains is presented. Bayesian inference is used to deduce the probability distribution of the unknown crack parameters conditional on the available strain data and Markov Chain Monte Carlo (MCMC) sampling is employed to explore the resulting distribution. Surrogate modeling is used to replace the computational mechanics model with a more efficient data-driven model to provide computational speedup in the approach. These points are elaborated on in detail in the subsequent subsections.

2.1. Preliminaries

In this study, the description of damage considered is a four-dimensional array of unknowns describing a straight crack in a panel under a prescribed displacement Δu (Figure 1)

$$\mathcal{C} = [x, y, a, \theta], \tag{1}$$

where (x, y) denotes the coordinates of the center of the crack and a and θ denote the crack length and orientation (*i.e.*, angle with respect to the x-axis), respectively. The measurement data used to inversely estimate the crack parameters are an array of m strains recorded throughout the domain

$$\mathcal{D} = \{\hat{S}_i\}_{i=1}^{m} \tag{2}$$

where $\hat{S}_i$ is the i^{th} strain measurement. Note that $\hat{S}_i$ can represent any one of the surface strain components $\{\hat{\epsilon}_{xx}, \hat{\epsilon}_{yy}, \hat{\gamma}_{xy}\}$ and multiple components can typically be measured at each sensor location.

The feasibility of strain-based diagnosis is predicated on the availability of a model $\mathcal{M}$ (*e.g.*, finite element analysis) with adequate predictive capabilities of strains $\{S\}$ in a component with an arbitrary crack $\mathcal{C}$

$$\{S_i\}_{i=1}^{m} = \mathcal{M}(\mathcal{C}). \tag{3}$$

Here, it is assumed that there is a one-to-one correspondence between the computed strain array $\{S\}$ and measurement data $\{\hat{S}\}$ through appropriate postprocessing of the model results. It is further assumed that this model has been appropriately calibrated and encompasses the appropriate geometry, boundary conditions, and material parameters for the component being analyzed, *e.g.*, the only variables changing during each new evaluation are the crack parameters.

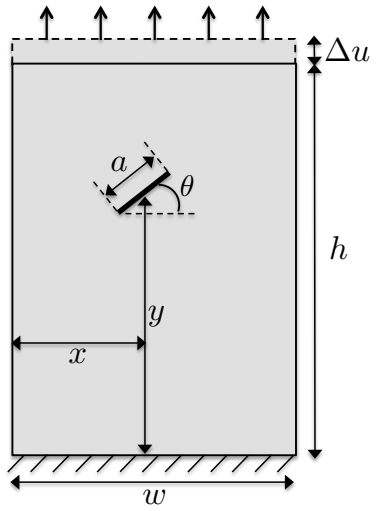

Figure 1. Diagram of the problem domain and crack parameterization considered for damage diagnosis.

Letting $\mathcal{M}_i(\mathcal{C}) \equiv S_i$, the following error metric between the measured strain data and corresponding computed strains can be defined as

$$Q(\mathcal{C}) = \sum_{i=1}^{m} \|\hat{S}_i - \mathcal{M}_i(\mathcal{C})\|^2 \tag{4}$$

where a lower value of $Q(\mathcal{C})$ ideally indicates a current estimate of $\mathcal{C}$ that is near the true crack that resulted in the measurement data $\mathcal{D}$. In this way, a typical deterministic model-based SHM approach (Krishnamurthy & Gallegos, 2011; Hochhalter et al., 2016) estimates $\mathcal{C}$ by minimizing Equation 4 using gradient-based or global optimization techniques, the so-called least squares estimator

$$\mathcal{C}^{LS} = \arg\min_{\mathcal{C}} Q(\mathcal{C}) \tag{5}$$

The primary drawback from such deterministic methods for diagnosis and inverse problems in general is that $\mathcal{C}^{LS}$ provides only a point estimate of the unknowns without rigorously quantifying the impact of model and measurement uncertainties. A suitable regularization strategy must also be chosen and tuned in an effort to rectify the well known ill-posedness of the inverse problem (Isakov, 1998) (*e.g.*, infinitely many solutions may exist).

2.2. Bayesian Inference

In the Bayesian inference approach to damage diagnosis used herein, the objective is to formulate the probability distribution of the unknown crack parameters $\mathcal{C}$ conditional on the measured strain dataset $\mathcal{D}$. This probability distribution $p(\mathcal{C}|\mathcal{D})$, referred to as the posterior probability density function, is given according to Bayes' formula:

$$p(\mathcal{C}|\mathcal{D}) = \frac{p(\mathcal{D}|\mathcal{C})p(\mathcal{C})}{p(\mathcal{D})} \tag{6}$$

which combines any *a priori* knowledge of the crack parameters through a prior density function $p(\mathcal{C})$ with the information provided by the measurement data through the likelihood function $p(\mathcal{D}|\mathcal{C})$. The normalizing constant, $p(\mathcal{D})$, is not required for numerical exploration of the posterior probability and so Equation (6) can be expressed as

$$p(\mathcal{C}|\mathcal{D}) \propto p(\mathcal{D}|\mathcal{C})p(\mathcal{C}) \tag{7}$$

The prior density function $p(\mathcal{C})$ can be a powerful tool for inserting an analyst's practical insight into the Bayesian inference approach. For example, identification of "hot spots" and stress concentrations can provide information on expected damage location, prognostic tools can yield estimates of future anticipated crack length, and engineering judgement can determine the likely orientation of a crack given the load state. From a mathematical point of view, prescribing such an informative prior density function $p(\mathcal{C})$ provides a means to regularize the inverse problem. In the absence of any reliable *a priori* knowledge, however, a non-informative (*e.g.*, uniform probability) prior density function can be chosen as to avoid any inaccurate biasing of the predictions.

The likelihood function $p(\mathcal{D}|\mathcal{C})$ models the discrepancy between the measured strain data and the corresponding values computed with the model. To obtain an expression for $p(\mathcal{D}|\mathcal{C})$, the following common assumption is made on the relationship between measured and computed strains

$$\hat{S}_i = \mathcal{M}_i(\mathcal{C}) + \delta_i, \quad \delta_i \sim N(0, \sigma) \tag{8}$$

That is, the measurement data are polluted with errors δ_i that are treated as a sequence of independent, identically distributed (iid) samples drawn from a zero-mean Gaussian distribution with variance σ^2 (interpreted as the noise level). The iid assumption yields the following expression for likelihood function

$$\begin{aligned} p(\mathcal{D}|\mathcal{C}) &= \prod_{i=1}^{m} p(\hat{S}_i|\mathcal{C}) \\ &= \frac{1}{(2\pi\sigma^2)^{m/2}} \exp\left(-\frac{1}{2\sigma^2} Q(\mathcal{C})\right) \end{aligned} \tag{9}$$

Here, it is clear that as the error between computed and measured strains (Equation (4)) increases, the value of the likelihood function (and hence posterior probability in Equation (7)) decreases and vice versa. The rate of increase/decrease in probability here is governed by σ^2.

An advantage of adopting a Bayesian approach to damage diagnosis is its inherent flexibility for modeling and inferring additional system parameters which may be difficult to prescribe *a priori* with sufficient certainty. In this work, this capability is demonstrated for the noise level parameter σ^2 as well as the applied displacement Δu. Using the product probability law (*i.e.*, $P(A|B) = P(A,B)P(B)$), the posterior probability distribution (7) can be modified to include the noise level

$$p(\mathcal{C}, \sigma^2|\mathcal{D}) \propto p(\mathcal{D}|\mathcal{C}, \sigma^2)p(\mathcal{C})p(\sigma^2) \tag{10}$$

or the prescribed displacement

$$p(\mathcal{C}, \Delta u|\mathcal{D}) \propto p(\mathcal{D}|\mathcal{C}, \Delta u)p(\mathcal{C})p(\Delta u). \tag{11}$$

For Equations 10 and 11, the prior distributions $p(\sigma^2)$ and $p(\Delta u)$ are introduced to complete the formulation. Note that the common choice for $p(\sigma^2)$, also adopted in this work, is the use of the inverse-gamma distribution. For the Gaussian noise assumption made in Equation 8, the inverse-gamma distribution for $p(\sigma^2)$ represents a *conjugate prior* which has algorithmic benefits for subsequent MCMC sampling (see (Nichols et al., 2010) for more details). While a uniform distribution is chosen in this work for $p(\Delta u)$, it is conceivable that a more informative prior distribution could be generated in practice through load monitoring.

Note that when Δu is treated as unknown, this parameter effectively appears as an additional input to the model in Equation 3 (*i.e.*, $\mathcal{M}(\mathcal{C}, \Delta u)$). Since linear elastic FE modeling is considered, however, the strains at the sensors for any new prescribed displacements Δu^* can be obtained by simply scaling previously computed model values

$$\mathcal{M}(\mathcal{C}, \Delta u^*) = \left(\frac{\Delta u^*}{\Delta u}\right) \mathcal{M}(\mathcal{C}, \Delta u). \tag{12}$$

This approach significantly reduces the computational

cost of the surrogate modeling and sampling processes to follow when considering an unknown applied displacement.

2.3. Surrogate Modeling

Surrogate modeling relies on the (*offline*) pre-computation and storage of input-output pair datasets from an original computational model in an effort to replace it during (*online*) analysis by a more efficient data-driven model. The approach is highly effective in reducing analysis times for Bayesian inference approaches that require repeated evaluation of computationally intensive models (Meeds & Welling, 2014; Warner & Hochhalter, 2016). Furthermore, with a sufficient amount of pre-computed data and an effective regression/interpolation algorithm, a high degree of accuracy with respect to the original model can be maintained.

In the strain-based damage diagnosis application considered here, a set of T crack parameter arrays $\{\mathcal{C}^{(k)}\}_{k=1}^{T}$ is first selected. Then, the model strains corresponding to all m measurement data (Equation (3)) are computed and stored for each predefined crack

$$\mathcal{M}_j^{(k)} \equiv \mathcal{M}_j(\mathcal{C}^{(k)}),\ k = 1, ..., T \tag{13}$$

for $j = 1, ..., m$. The result is the following $T \times (d + m)$ input-output dataset

$$\mathcal{S} = \{\mathcal{C}^{(k)}; \mathcal{M}_1^{(k)}, ..., \mathcal{M}_m^{(k)}\}_{k=1}^{T}, \tag{14}$$

The objective of surrogate modeling is to now utilize the data $\mathcal{S}$ to predict the value of strains for new crack parameters $\mathcal{C}^* \notin \mathcal{S}$ without requiring an additional evaluation of the original model $\mathcal{M}$. From a machine learning perspective, $\mathcal{S}$ is the training data and a variety of off-the-shelf regression and interpolation algorithms can be utilized to directly infer the input-output mappings. These algorithms, appropriately trained with the data $\mathcal{S}$, form the surrogate models

$$\widetilde{\mathcal{M}}_j : \mathcal{C} \rightarrow \mathcal{M}_j \text{ for } j = 1, ..., m \tag{15}$$

which can be used to replace the original model in the posterior probability distribution (Equation (7)).

A couple of remarks about the surrogate modeling process are worth noting. First, the size T of the training data set has a lower limit based on accuracy requirements and a practical upper limit based on the computational expense of the original model $\mathcal{M}$, the computational resources available, and the training complexity and memory requirements of the regression/interpolation algorithm used. In this work, a testing data set $\hat{\mathcal{S}}$ of randomly generated points

$$\hat{\mathcal{S}} = \{\hat{\mathcal{C}}^{(n)}; \hat{\mathcal{M}}_1^{(n)}, ..., \hat{\mathcal{M}}_m^{(n)}\}_{n=1}^{P}, \tag{16}$$

is used to evaluate surrogate model accuracy for both different training dataset sizes and different learning algorithms. The assessment is based on the relative error between the surrogate and original models when predicting the test data

$$\Delta_j = \frac{1}{P} \sum_{n=1}^{P} \frac{|\widetilde{M}_j(\hat{\mathcal{C}}^{(n)}) - \hat{\mathcal{M}}_j^{(n)}|}{|\hat{\mathcal{M}}_j^{(n)}|} \tag{17}$$

It is also worth pointing out that the T model evaluations and the training of the m surrogate models is an offline cost associated with the diagnosis framework. That is, the computational burden of generating the surrogate models is a single upfront cost that then permits an arbitrary number of efficient damage diagnoses to be conducted by rapidly evaluating $\widetilde{\mathcal{M}}_j$ during the analyses. Furthermore, the T executions of the finite element method (FEM) simulation are completely independent of each other, and can therefore be run in parallel on as many computer processors as are available.

2.4. Markov Chain Monte Carlo Sampling

In the Bayesian inference approach to inverse problems, Markov Chain Monte Carlo (MCMC) (Gelman et al., 2013) sampling methods are the common choice for exploring the resulting posterior probability distribution (Equation (7)). MCMC generates iid samples from a target probability distribution by constructing a Markov chain that, by design, is guaranteed to have a stationary distribution that matches that of the target. For the damage diagnosis framework here, N samples of the unknown crack parameters $\mathcal{C}$ are drawn from the posterior probability distribution $p(\mathcal{C}|\mathcal{D})$ using MCMC which can then be used to construct empirical probability distributions, creditability intervals, and moment estimates for $\mathcal{C}$.

Algorithm 1 summarizes the most basic form of MCMC, the Metropolis algorithm (Gamerman & Lopes, 2006). Here, the method simply draws a trial sample $\mathcal{C}^t$ at each iteration from a *proposal distribution* $q(\mathcal{C}^t|\mathcal{C}^{(j-1)})$, and then decides whether to accept or reject this sample based on the *acceptance probability*, $A(\mathcal{C}^t, \mathcal{C}^{(j-1)})$. The Metropolis algorithm assumes that the proposal distribution is symmetric, where a common choice is a Gaussian

Algorithm 1 The Metropolis MCMC Algorithm

Initialize $\mathcal{C}^{(0)}$
for $j = 1 : N$ **do**
  Sample $u \sim \text{Uniform}(0, 1)$
  Sample $\mathcal{C}^t \sim q(\mathcal{C}^t|\mathcal{C}^{(j-1)})$
  if $u < A(\mathcal{C}^t, \mathcal{C}^{(j-1)}) = \min\{1, \frac{p(\mathcal{C}^t|\mathcal{D})}{p(\mathcal{C}^{(j-1)}|\mathcal{D})}\}$ **then**
    $\mathcal{C}^{(j)} = \mathcal{C}^t$
  else
    $\mathcal{C}^{(j)} = \mathcal{C}^{(j-1)}$
  end if
end for

distribution centered at the previous sample

$$q(\mathcal{C}^t|\mathcal{C}^{(j-1)}) = N(\mathcal{C}^{(j-1)}, \Sigma_q) \tag{18}$$

where Σ_q is the user-specified covariance matrix.

While the Metropolis algorithm is straightforward to implement, tuning of the algorithm (namely, the selection of an appropriate Σ_q) for efficient convergence and appropriate sample acceptance rate is notoriously difficult (Gamerman & Lopes, 2006) . Moreover, the posterior probability distributions formulated with Bayesian inference are often multimodal and grow in complexity with the number of unknown parameters. As such, it can take an extremely large number of samples to sufficiently explore the posterior probability distribution in addition to a lengthy initial *burn-in* period to allow the Markov chain to reach its stationary distribution.

In an effort to overcome these difficulties, the Delayed-Rejection Adaptive Metropolis Algorithm (DRAM) (Haario et al., 2006) is adopted in this work to sample the posterior probability distribution (Equation (7)) more effectively. The adaptive component of the algorithm allows for online tuning of Σ_q based on past samples to better reflect the target probability distribution. Delayed rejection allows for multiple stages of proposal samples at each iteration, which can help explore multimodal distributions more effectively by taking bolder (*i.e.*, larger) proposal steps in the initial stage followed by a more conservative step with a higher likelihood of acceptance. The reader is referred to (Haario et al., 2006) for more details on the DRAM algorithm.

While the DRAM algorithm can provide improved convergence of the sampling process, a poor initial guess $\mathcal{C}^{(0)}$ for the algorithm can still result in a time-consuming burn-in period, limiting it's effectiveness. In this work, a simple enhancement is introduced that utilizes the previously stored surrogate model training data to generate the initial guess in a high probability region of the posterior distribution, effectively reducing the required burn-in period. As a preprocessing step for the damage diagnosis process, the least squares estimator (Equation (4)) is computed over the surrogate model training data set (Equation (14)) as the initial guess for MCMC

$$\mathcal{C}^{(0)} = \underset{\mathcal{C} \in \mathcal{S}}{\arg\min}\, Q(\mathcal{C}) \tag{19}$$

By only considering the precomputed training grid values, this computation can be done rapidly as it does not require any additional model evaluations. While multimodal distributions may still pose a challenge, Equation (19) is a simple and systematic way to generate a good starting point for the DRAM algorithm and can help yield shorter burn-in periods.

Note that while strain-based crack identification is the focus of the current study, the approach formulated herein is general for $\mathcal{C}$, $\mathcal{D}$, $\mathcal{M}$, and $\widetilde{\mathcal{M}}$. The primary assumption that must hold when substituting components in the framework is the availability of a computational model with adequate predictive capability of the measured data after appropriate calibration. Note that in practice, however, higher order descriptions of damage will be limited by the sensitivity of the additional parameters to the measured quantity used for diagnosis.

3. Experimental Validation

The implementation of the Bayesian damage diagnosis framework, including surrogate model development and MCMC sampling, was carried out in Python (Python Software Foundation, 2016). The performance of the framework through experimental validation is now demonstrated. A description of the strain measurement data acquired for diagnosis is provided followed by the development and validation of the surrogate models used. Next, the diagnosis framework is applied to one example of damage localization followed by another demonstrating general damage characterization (location, size, orientation) in thin metal sheets. Finally, the impact of specifying informative prior distributions with the Bayesian framework as well as its ability to infer an unknown prescribed displacement during diagnosis is illustrated.

3.1. DIC Strain Data

Two cracked thin sheet specimens of Aluminum Alloy 2024 (AA2024) were considered for experimental validation of the diagnosis framework, one with a flat crack (*i.e.*, oriented 0° from the x axis) used to test damage localization and the other with an an-

gled crack to test full crack characterization. Full field strain data was acquired with digital image correlation (DIC) using the VIC3D (Correlated Solutions Inc., 2012) software. The width and height of the specimens were 3.93in and 8.73in, respectively. The crack parameters were $[x_{\text{flat}}, y_{\text{flat}}, a_{\text{flat}}, \theta_{\text{flat}}] = [1.81\text{in}, 4.53\text{in}, 0.67\text{in}, 0\text{rad}]$ for the flat crack specimen and $[x_{\text{angled}}, y_{\text{angled}}, a_{\text{angled}}, \theta_{\text{angled}}] = [1.83\text{in}, 4.29\text{in}, 0.78\text{in}, -0.82\text{rad}]$ for the angled crack specimen. The strain fields recorded with DIC are displayed in Figure 2, showing the ϵ_{XX} and ϵ_{YY} strain components for both test specimens. Note that the ϵ_{XY} component of strain was not considered as measurement data for diagnosis in this study.

The motivation behind gathering full field strain data using DIC was that measurement ("sensor") locations could be freely chosen in order to test the diagnosis accuracy as the distance between the measured data and damage was varied. Four different sensor arrangements were tested in the diagnosis examples to follow, shown in Figure 3 along with the two crack configurations considered. Each arrangement was composed of two separate horizontal arrays of sensors with increasing distance between them (1.47", 3.25", 5.02", and 6.79"). Fourteen measurement locations with two recorded strain components per location were considered ($m = 24$) for each sensor arrangement.

The software used for FE modeling in this study was the Scalable Implementation of Finite Elements by NASA (ScIFEN) (Warner, Bomarito, Heber, & Hochhalter, 2016) parallel FE code. A Young's Modulus $E = 10.6Msi$ and a Poisson's ratio $\nu = 0.33$ for AA2024 were considered known and deterministic. A simple calibration of the FE model to the DIC data was performed by treating the prescribed displacement Δu as the single free parameter. For each test specimen, the measured crack parameters were inserted into the FE model and Δu was adjusted such that the far field value of ϵ_{YY} at a location sufficiently far from the damage (≈ 1 in. from the upper boundary) agreed between the model and the DIC data. The resulting values for Δu for the flat and angled crack specimens were 0.028in and 0.032in, respectively.

To gauge the error/noise level between the calibrated FEM model and the DIC data, the strains were compared on a grid of 325 points throughout the domain. The distribution of absolute errors between FEM and DIC strains are shown in Figure 4 for the flat (a) and angled (b) crack specimens along with a fitted Gaussian distribution to the errors. The Gaussian noise model used in Equation 8 is shown to be a reasonably accurate assumption, more so for the flat crack specimen. The FE model predictions show a positive bias for the angled crack specimen strains, which could be a result of the simplified calibration procedure used. Note that the empirical standard deviations noted in Figures 4(a) and 4(b) will be used to prescribe the variance parameter σ^2 during the Bayesian diagnosis process in the experimental validation study to follow.

3.2. Surrogate Model Development

Two separate sets of surrogate models were developed for the flat crack and angled crack specimen since the former was used to demonstrate damage localization ($\mathcal{C}_{\text{flat}} = [x, y] \in \mathbb{R}^2$, with $a = 0.67$in and $\theta = 0$rad) while the latter was used for full crack characterization ($\mathcal{C}_{\text{angled}} = [x, y, a, \theta] \in \mathbb{R}^4$). For both specimens, surrogate models were constructed and stored for each measurement in the sensor arrays considered (Figure 3) that were capable of mapping new values of $\mathcal{C}_{\text{flat}}$ and $\mathcal{C}_{\text{angled}}$ directly to the resulting strain (Equation 15). Several different machine learning algorithms from the `scikit-learn` (Buitinck et al., 2013) and `SciPy` (Jones, Oliphant, Peterson, et al., 2001–) Python modules were compared to obtain a surrogate model with an optimal balance of prediction accuracy and efficiency.

First, training datasets $\mathcal{S}$ (Equation 14) were generated using the ScIFEN FE code according to Equation 13. For the case of damage localization in the flat crack specimen, several uniform training grids $\{\mathcal{C}_{\text{flat}}^{(k)}\}_{k=1}^{T}$ were considered from $T = 450$ to $T = 5000$ to study the accuracy and efficiency of the machine learning algorithms for increasing training data size. Only one training grid with $T = 32076$ was generated for the angled crack specimen due to the added computational expense of the increased dimension of the input space $d = 2$ to $d = 4$. Additionally, two test datasets $\hat{\mathcal{S}}$ (Equation 16) were generated from 500 and 1000 randomly selected values of $\mathcal{C}_{\text{flat}}$ and $\mathcal{C}_{\text{angled}}$, respectively, to verify the accuracy of the trained surrogate models. The bounds for the parameters for training and testing were specified as

$$x \in [0.64, 3.18]\text{in} \tag{20}$$

$$y \in [0.64, 7.94]\text{in} \tag{21}$$

$$a \in [0.20, 1.19]\text{in} \tag{22}$$

$$\theta \in [-\pi/2, \pi/2]\text{rad} \tag{23}$$

where the bounds for x, y, and a were chosen such that the entire crack would always be contained within the geometry (*i.e.*, edge cracks were not considered).

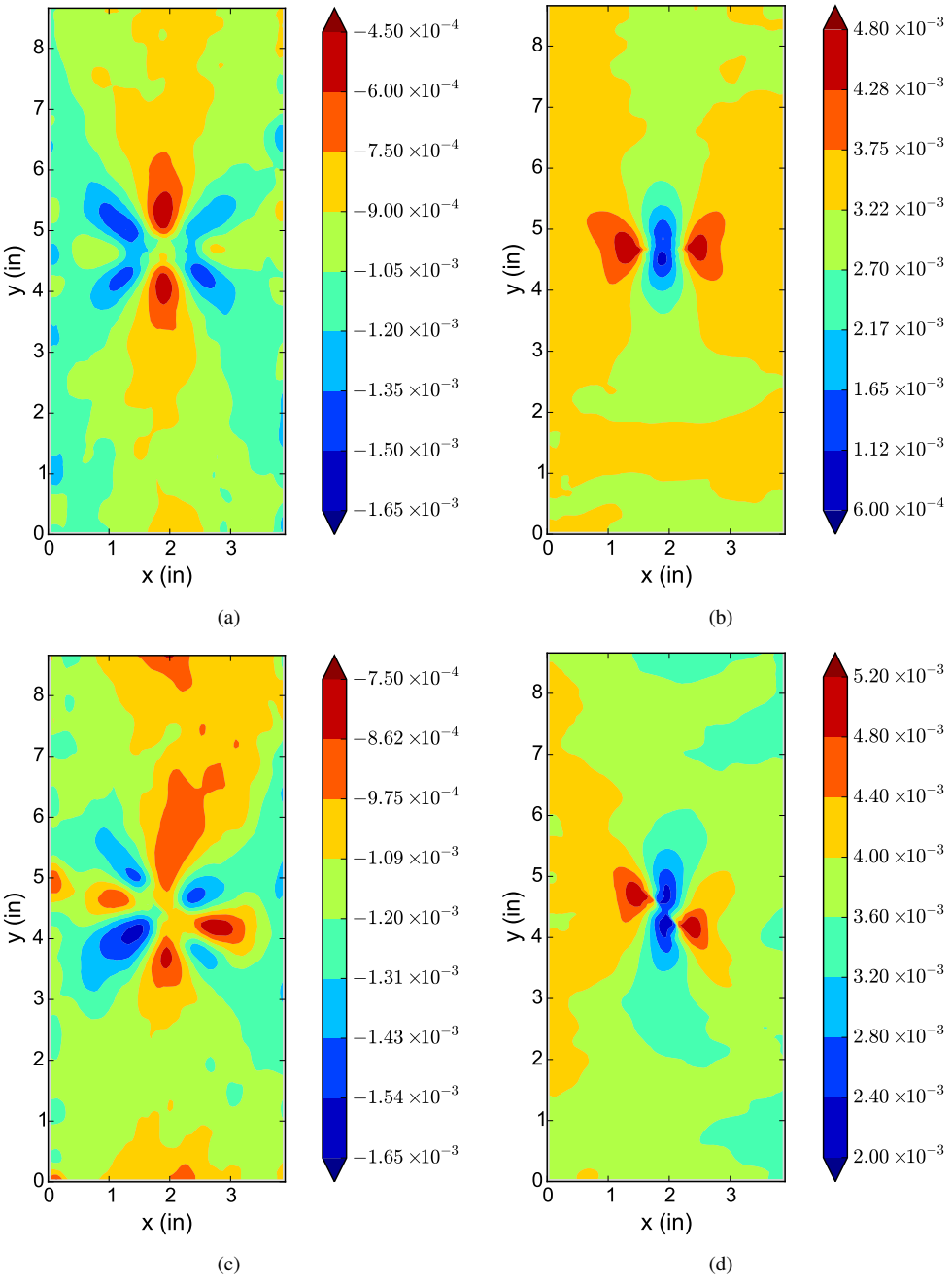

Figure 2. DIC strain data for flat and angled crack specimens: (a) ϵ_{XX} and (b) ϵ_{YY} for the flat crack specimen, and (c) ϵ_{XX} and (d) ϵ_{YY} for the angled crack specimen.

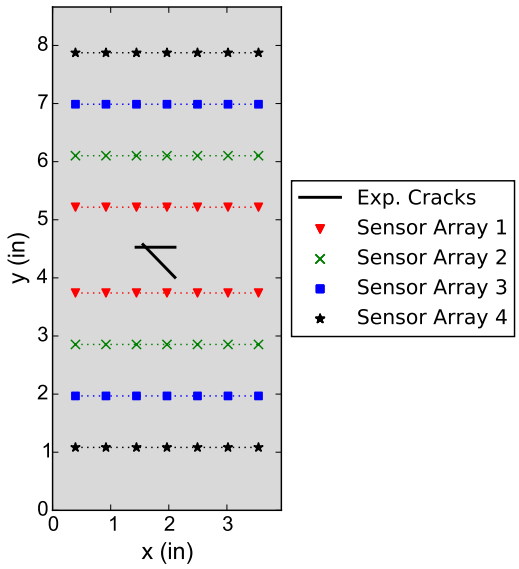

Figure 3. Diagrams of the effective sensor arrays tested and the cracks from the flat and angled crack specimens.

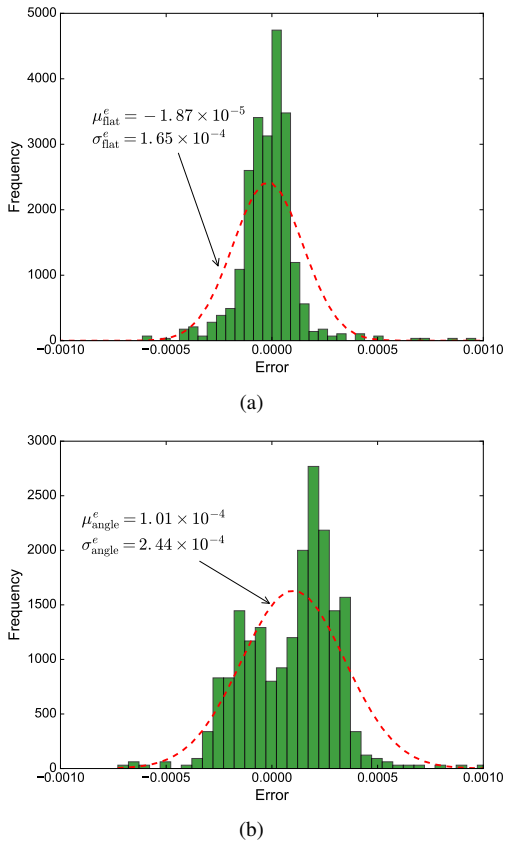

Figure 4. Histogram of errors between DIC and FE strains with fitted Gaussian distributions, for the a) flat and b) angled crack specimen.

Four separate FE simulations were run simultaneously to generate the training and testing datasets with each individual simulation run in parallel on four processors, for a total of 16 processors used. The CPU times for each FE model execution varied between 25 and 45 seconds depending on the crack geometry and computational mesh, resulting in a total run time of approximately 5 days to generate all necessary data for surrogate model development.

Surrogate models for the flat crack specimen were generated using linear regression, nearest neighbors, and Gaussian process algorithms from `scikit-learn` and a multi-linear interpolation algorithm from `SciPy`. Free parameters for the nearest neighbors and Gaussian process models were tuned using cross-validation. A comparison of algorithm performance for increasing training dataset sizes is shown in Figure 5. Figure 5(a) shows the average relative error over the testing dataset (Equation 17) while Figures 5(b) and 5(c) compares the training and prediction times for the different models tested, respectively.

The linear regression models performed most poorly both in terms of accuracy and prediction times, which are the most important metrics for online analysis (surrogate model training is considered an off-line cost of the framework). While the remaining three algorithms showed comparable accuracy in predicting the test data (all near or below 1% average error for $T = 5000$), the linear interpolation models were significantly faster in terms of prediction efficiency. The nearest neighbor models, however, demonstrate significantly lower training times and near-constant scaling of prediction times with respect to dataset size, indicating that they excel when a large amount of training data are used. Note that all algorithms exhibit prediction times that are orders of magnitude faster than computing the strains using FE simulation. Based on the overall performance in Figure 5, however, the linear interpolation surrogate models were chosen for the damage localization study in the flat crack specimen.

For the angled crack specimen, only the nearest neighbor and linear interpolation approaches were considered due to the poor accuracy of the linear regression models and the lengthy training times of the Gaussian process models for larger training datasets observed in Figure 5. The performance of the algorithms in terms of accuracy and efficiency is displayed in Table 1. The linear interpolation models have slightly less error in predicting the testing data but scale significantly worse in terms of prediction and training times to higher dimensional inputs

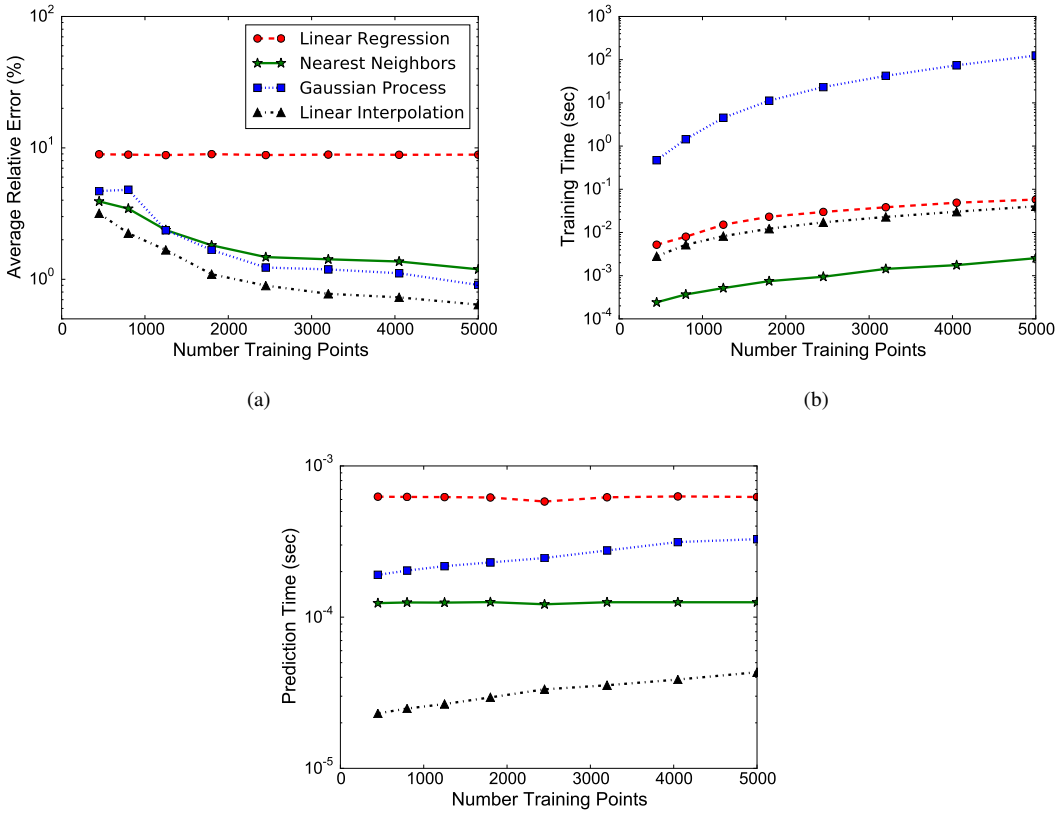

Figure 5. Performance comparison of four different surrogate modeling algorithms for the damage localization problem in terms of a) relative error, b) training time, and c) prediction time.

($d = 4$) and larger amounts of training data. Based on the difference of over two orders of magnitude in prediction times and comparable accuracy, the nearest neighbor models are selected over linear interpolation for the general crack characterization study in the angled crack specimen.

3.3. Damage Localization

The Bayesian damage diagnosis framework was first applied to the problem of damage localization in the flat crack specimen. The DRAM MCMC algorithm described in Section 2.4 was implemented in Python to sample the posterior probability distribution $p(\mathcal{C}|\mathcal{D})$ and estimate $\mathcal{C}_{\text{flat}}$. Two cases were considered: 1) a prescribed noise level using the posterior distribution in Equation 7 with σ^2 estimated from Figure 4(a), and 2) an inferred noise level using the form of posterior distribution in Equation 10, estimating σ^2 during the sampling process. A uniform distribution was used for the prior probability $p(\mathcal{C})$, simply enforcing the bounds in Equations 20 - 21 (*i.e.*, 0 probability if either parameter falls outside the bounds in a given sample). The linear interpolation surrogate models described in the previous section were used to accelerate the evaluation of $p(\mathcal{C}|\mathcal{D})$ during sampling. DIC strain data from each of the four sensor arrays in Figure 3 were tested individually to compare the impact of measurement location on the resulting damage location estimates.

For all of the damage diagnosis results presented in this study, 11000 total samples were drawn using the DRAM algorithm. The first 1000 samples were discarded for the burn-in period after which a thinning interval of 10 was applied to reduce autocorrelation, yielding 1000 samples to produce estimates of damage location probability. Initial guesses for sampling were generated automatically using the approach indicated in Equation 19. The initial covariance matrix Σ_q for the proposal distribution (Equation 18) was chosen such that the variance for each parameter was 10% of its corresponding bounds in Equations 20 - 23, after which it was adapted during sampling according to the DRAM algorithm. The sample acceptance rate for the damage localization results presented in this section was between 54.4% and 58.6% while the average solution time for all cases was just 13.5 seconds.

Figure 6 shows the resulting crack location probability contours in the case of prescribed noise level σ^2 for each of the sensor arrays. It can be seen that sensor array 1 6(a), which is closest to the crack, provides an accurate estimate of the true crack location with high certainty. The accuracy of the estimates (the agreement between the true crack and highest estimated probability) decrease with increasing distance between the sensor arrays used, as expected. The Bayesian diagnosis framework effectively captures the growing uncertainty in estimates, however, as indicated by the growing spread in the probability distributions. Furthermore, even the probability distribution produced by 6(d), which is farthest from the crack, has a mode which is reasonably close to the true crack location, albeit with a high degree of uncertainty.

The difference in performance between using a prescribed versus inferred noise level σ^2 during diagnosis can be seen in Figure 7, showing the marginal probability distributions of the x and y coordinates of crack location for each case. While the accuracy is comparable in each case, the uncertainty appears to be underestimated when inferring σ^2 during the sampling process. This can be noted from the decreased spread in probability in Figures 7(b) and 7(d). More specifically, the mean estimates for σ^2 obtained from DRAM for sensor arrays 1-4 were $[1.41 \times 10^{-8}, 6.77 \times 10^{-9}, 6.77 \times 10^{-9}, 1.33 \times 10^{-8}]$ compared to the prescribed value of 2.71×10^{-8} obtained by comparing the FE and DIC strains directly. As observed previously in Figure 6, the increase in uncertainty and decrease in accuracy is clearly shown again in Figure 7 as the distance between sensors increases from array 1 to array 4.

3.4. General Crack Characterization

The performance of the proposed diagnosis framework is now illustrated for general crack characterization in the angled crack specimen. That is, the probability distribution $p(\mathcal{C}_{\text{angled}}|\mathcal{D}) = p(x, y, a, \theta|\mathcal{D})$ for unknown crack location, size, and orientation was estimated using each sensor array of DIC strains in Figure 3. Again, both the prescribed and inferred noise level cases were tested where the prescribed value of σ^2 was estimated from Figure 4(b). Nearest neighbor surrogate models were used to accelerate the sampling process for crack characterization following the developments in Section 3.2. The DRAM sampling parameters remained unchanged from those provided for the damage localization results in the previous section and a uniform distribution was used again for the prior probability $p(\mathcal{C})$. The sample acceptance rate for the results to follow was between 35.7% and 53.7% for all cases while the average solution time was 64.4 seconds. Note the slower execution time versus damage localization is a result of an increase in prediction time of the nearest neighbor surrogate mod-

Method	Relative Error	Training Time	Prediction Time
Nearest Neighbors	3.84%	3.80e-2 sec	1.38e-4 sec
Linear Interpolation	2.89%	76.5 sec	2.15e-2 sec

Table 1. Performance comparison for the full damage characterization surrogate models.

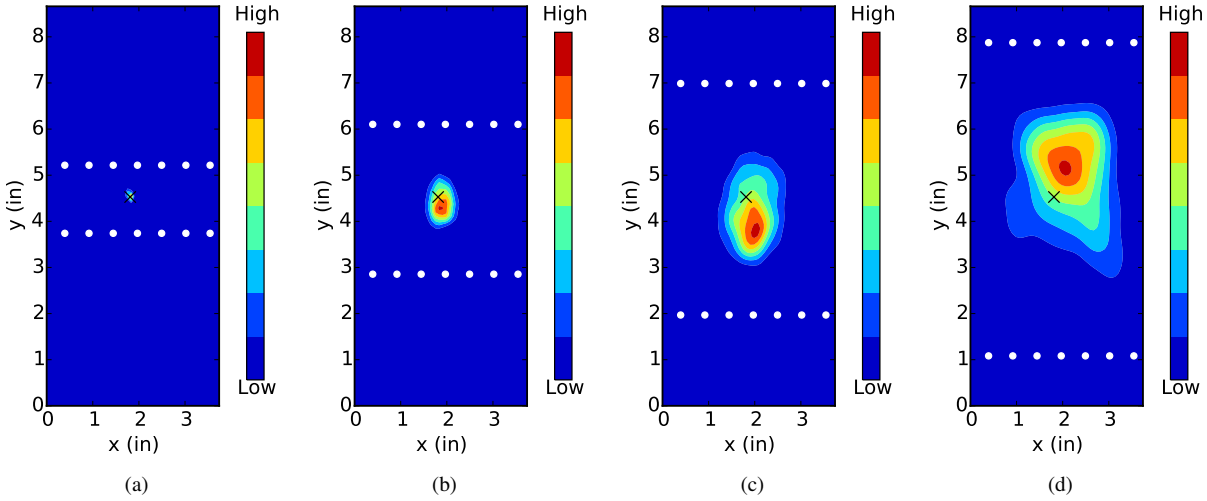

Figure 6. Crack location probability contours using the different sensor arrays from Figure 3 (denoted by white circles).

els trained with a larger training dataset and higher input dimension.

The results for general crack characterization for both the prescribed and inferred noise level cases using each of the four sensor arrays considered are shown in Figure 8. Here, the estimated marginal probability distributions for x, y, a, and θ are displayed along with the true values of these parameters from the angled crack specimen. Again, the trend of decreasing accuracy and increasing uncertainty is observed with increasing distance between sensor arrays used for diagnosis. The results for the case of prescribed noise level are more accurate and the uncertainty tends to be slightly underestimated with the noise level is inferred during sampling. In particular, the estimated marginal distributions produced using sensor arrays 1 and 2 (closest to the damage) generally have probability modes that are near the true values of the crack parameters with relatively low uncertainty. On the other hand, for the inferred noise case and measured strains from sensor arrays 3 and 4 (farthest from the damage), the framework prescribes relatively low probability to the true parameter values. Viewing the relatively localized nature of the damage effects on the strain fields in Figure 2 and the locations of sensor arrays 3 and 4 in Figure 3, it can be inferred that there is not an adequate level of information in the measurement data to accurately infer the damage parameters in these cases.

3.4.1. Informative Prior Distributions

The damage diagnosis results presented so far have assumed uniform (*i.e.*, non-informative) prior probabilities $p(\mathcal{C})$ to provide an unbiased presentation of the framework. However, a primary strength of the Bayesian approach in practice is the ability to factor in engineering judgement and expert opinion during the inference process. This section briefly illustrates the impact of providing an informative prior probability distribution for the unknown parameters during crack characterization.

For the purposes of demonstration, a multivariate Gaussian prior distribution centered at the initial guess calculated using Equation 19 is chosen

$$p(\mathcal{C}) = N(\mathcal{C}^{(0)}, \gamma \text{diag}(\mathcal{C}^{(0)})) \tag{24}$$

where γ is a scaling factor controlling the amount of variance. This choice of prior effectively represents an inference approach that is a balance between deterministic least squares (Equation 5) and probabilistic Bayesian solutions where an emphasis between one or the other is controlled by γ. Note that in practice, $p(\mathcal{C})$ would be based on some *a priori* intuition about the nature of ex-

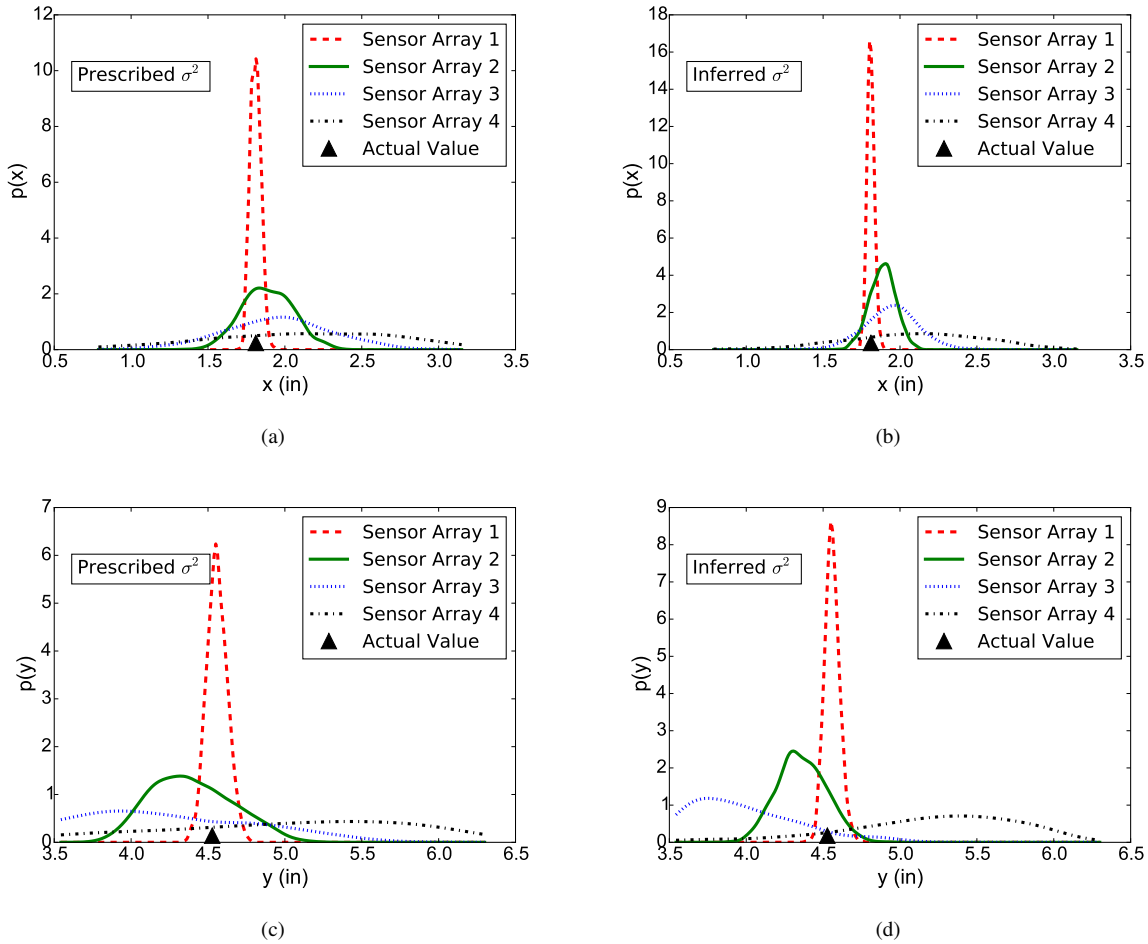

Figure 7. Marginal probability distributions of the x and y coordinates of crack location using a prescribed versus inferred noise level σ^2.

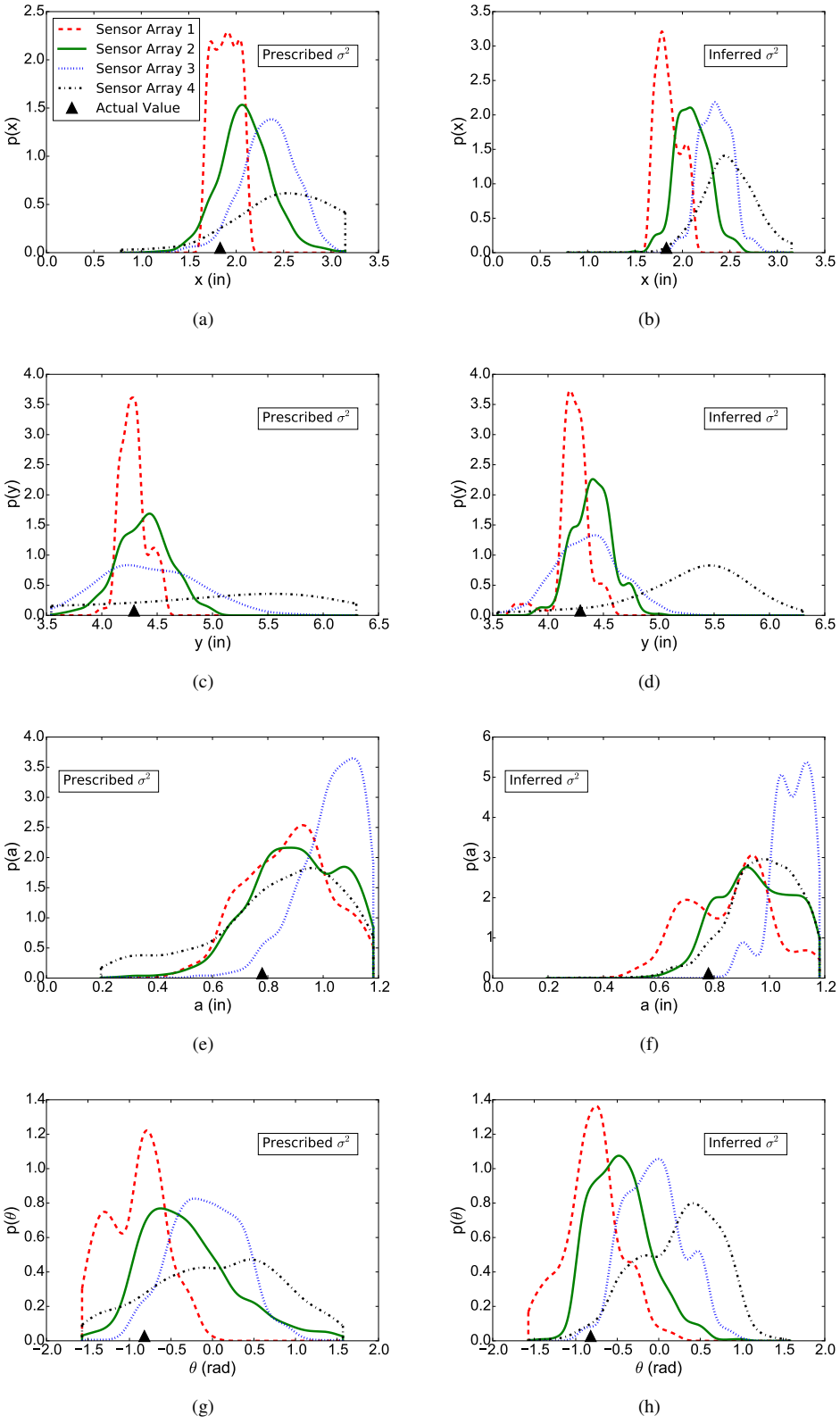

Figure 8. Marginal probability distributions of the crack parameters for the angled crack specimen using a prescribed versus inferred noise level σ^2.

pected damage and independent of the measurement data $\mathcal{D}$. Equation 24 is chosen here out of convenience and to simply demonstrate the prior probability modeling mechanism.

The DRAM sampling algorithm is used to sample the posterior probability distribution in Equation 7 with prescribed noise level, using the prior distribution in Equation 24 with $\gamma = 0.2$ and strain data from sensor array 3 (Figure 3). The resulting marginal distributions of the crack parameters are displayed in Figure 9, showing the prior probability, likelihood, and posterior distribution for each parameter. Note here that the likelihood is simply the posterior distribution from Figure 8 since these distributions are equivalent when using a uniform prior distribution. The effect on the resulting posterior distributions from prescribing an informative prior distribution is clear, where the impact is larger for the distributions of a and θ which were originally less accurate and more uncertain than x and y. The resulting crack parameter distributions are visibly a synthesis of the information provided individually by the likelihood and prescribed priors, which in this case yields more accurate estimates with less uncertainty. While this is a relatively contrived use case, the potential impact of incorporating *a prior* knowledge or assumptions through prior distributions with the Bayesian framework is apparent.

3.4.2. Unknown Boundary Condition

The ability of the Bayesian damage diagnosis framework to treat the prescribed displacement Δu as an additional unknown parameter is now briefly demonstrated. While the previous results have prescribed deterministic values for Δu based on the calibration described in Section 3.1, here its probability distribution is simultaneously estimated during diagnosis by sampling the modified posterior distribution in Equation 11. Damage diagnosis is carried out using sensor arrays 1 and 2 (Figure 3) with uniform distributions assumed for $p(\mathcal{C})$ and $p(\Delta u)$.

The resulting empirical distributions of Δu inferred during diagnosis are provided in Figure 10, comparing the estimates with each sensor array to the deterministic calibrated value from Section 3.1. The distributions of Δu showed a relatively high degree of certainty and good agreement with the previously used calibrated value of 0.032in. To quickly verify that the predictions of $\mathcal{C}$ have not been significantly affected by the additional unknown parameter, the $\%$ error in the sample mean for each crack parameter is compared for both the unknown Δu case here and the known Δu case from Section 3.4. The errors in the mean estimates, shown in Table 2 are comparable in both cases and are actually slightly lower overall for the unknown boundary condition case. These results demonstrate the ability of the framework to simultaneously estimate Δu during diagnosis and also indicate that the previously deterministic calibrated value may be slightly over-estimated from its true value.

4. CONCLUSION

In this study, a computationally-efficient, probabilistic damage diagnosis framework was presented and experimentally validated. Bayesian inference and MCMC sampling were used to perform both damage localization and characterization with associated quantification of uncertainties induced from measurement errors. Surrogate modeling was used to provide substantial computational speedup during the diagnosis process. While the proposed formulation is general for arbitrary component geometry, damage type, and sensor data, it was demonstrated on the problem of panel crack characterization using strain data determined from DIC. Different subsets of DIC data were used individually for analysis to test the effectiveness of strain-based diagnosis as the distance between the damage and measurement locations increased.

The ability of the framework to perform both probabilistic damage localization and characterization while effectively capturing the uncertainty in the predictions as the measurement locations were varied was demonstrated. Additional strengths of adopting a Bayesian approach were also illustrated, including the impact of specifying informative prior distributions on the damage predictions as well as the ability to infer an unknown noise level and prescribed displacement during diagnosis. Furthermore, the use of a surrogate model to replace a 3D FE model was shown to yield average analysis times of 13.5 and 64.4 seconds for damage localization and full damage characterization, respectively. While the accuracy and certainty of the diagnosis results naturally degraded as measurement locations were moved further from the damage, this study reinforced the potential for strain sensors to allow for effective local SHM of hot spots in components. Additionally, the framework, capable of providing full damage characterization with UQ and computational efficiency, encompasses the necessary characteristics to enable subsequent damage prognosis.

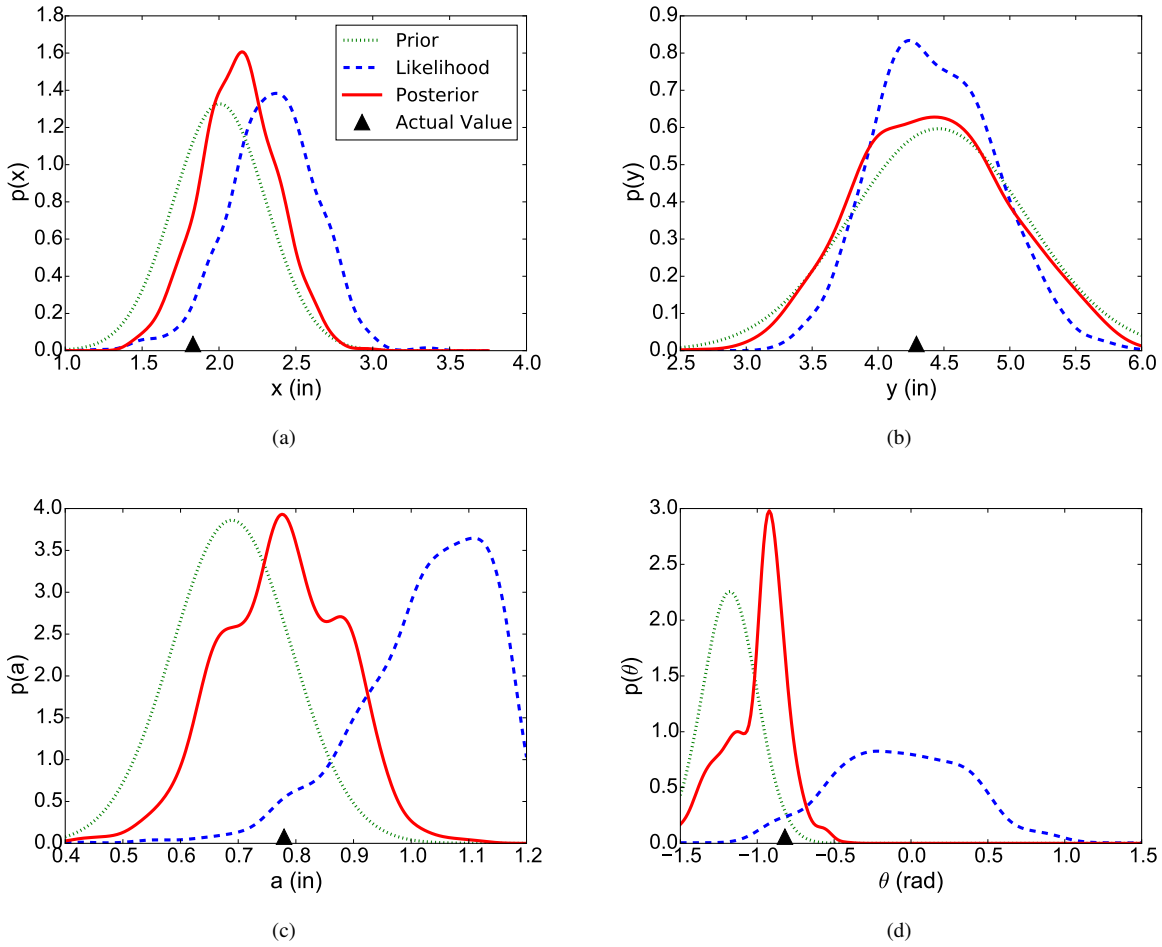

Figure 9. Marginal prior probability, likelihood, and posterior probability distributions of the crack parameters for the angled crack specimen.

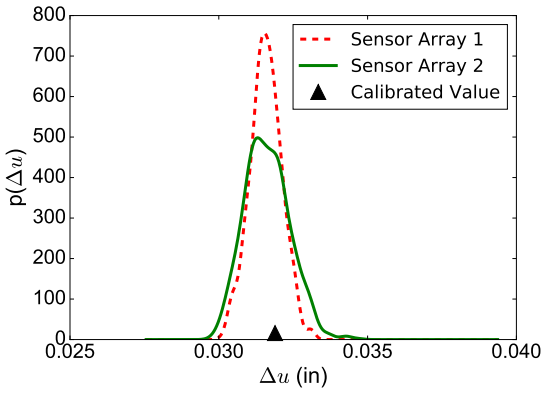

Figure 10. Marginal probability distributions of the applied boundary condition Δu inferred during crack characterization using sensor arrays 1 and 2.

REFERENCES

Barthorpe, R. J. (2010). *On model- and data-based approaches to structural health monitoring* (Unpublished doctoral dissertation). University of Sheffield.

Buitinck, L., Louppe, G., Blondel, M., Pedregosa, F., Mueller, A., Grisel, O., ... Varoquaux, G. (2013). API design for machine learning software: experiences from the scikit-learn project. In *Ecml pkdd workshop: Languages for data mining and machine learning* (pp. 108–122).

Correlated Solutions Inc. (2012). *Vic-3d.* Retrieved from `www.correlatedsolutions.com`

Farrar, C. R., & Worden, K. (2013). *Structural health monitoring: A machine learning perspective.* Wiley.

Gamerman, D., & Lopes, H. F. (2006). *Markov chain monte carlo: Stochastic simulation for bayesian inference* (Second ed.). Boca Raton, Florida: Chapman and Hall/CRC.

Gelman, A., Carlin, J. B., Stern, H. S., Dunson, D. B., Vehtari, A., & Rubin, D. B. (2013). *Bayesian data analysis* (Third ed.). Boca Raton, Florida: Chapman and Hall/CRC.

Haario, H., Laine, M., & Mira, A. (2006). Dram: Efficient adaptive MCMC. *Statistics and Computing*, *16*(4), 339-354.

Hochhalter, J. D., Krishnamurthy, T., Aguilo, M. A., & Gallegos, A. M. (2016). Strain-based damage determination using finite element analysis for structural health management. NASA/TM-2016-219186.

Huhtala, A., & Bossuyt, S. (2011). A bayesian approach to vibration based structural health monitoring with experimental verification. *Journal of Structural Mechanics*, *44*(4), 330-344.

Isakov, V. (1998). *Inverse problems for partial differential equations*. New York: Springer.

Jones, E., Oliphant, T., Peterson, P., et al. (2001–). *SciPy: Open source scientific tools for Python.* Retrieved from `http://www.scipy.org/`.

Katsikeros, C., & Labeas, G. (2009). Development and validation of a strain-based structural health monitoring system. *Mechanical Systems and Signal Processing*, *23*(2), 372 - 383.

Kehlenbach, M., & Hanselka, H. (2003, April). Automated structural integrity monitoring based on broadband lamb wave excitation and matched filtering. In *Proceedings of the 44th AIAA, ASME, ASCE, AHS, ASC Structures, Structural Dynamics, and Materials Conference.* Norfolk, VA.

Kim, J. T., & Stubbs, N. (2002). Improved damage identification method based on modal information. *Journal of Sound and Vibration*, *252*, 223-238.

Krishnamurthy, T., & Gallegos, A. M. (2011, April). Damage characterization using the extended finite element method for structural health management. In *52nd AIAA/ASME/ASCE/AHS/ASC Structures, Structural Dynamics, and Materials Conference 13th AIAA Non-Deterministic Approaches Conference.* Denver, CO.

Mal, A. K., Ricci, F., Banerjee, S., & Shih, F. (2005). A conceptual structural health monitoring system based on vibration and wave propagation. *Structural Health Monitoring*, *4*, 283-293.

Marzouk, Y. M., Najm, H. N., & Rahn, L. A. (2006). Stochastic spectral methods for efficient bayesian solution of inverse problems. *Journal of Computational Physics*, *224*, 339-354.

Meeds, E., & Welling, M. (2014). GPS-ABC: gaussian process surrogate approximate bayesian computation. *CoRR*, *abs/1401.2838*. Retrieved from `http://arxiv.org/abs/1401.2838`

Moore, E. Z., Murphy, K. D., & Nichols, J. M. (2011). Crack identification in a freely vibrating plate using bayesian parameter estimation. *Mechanical Systems and Signal Processing*, *25*, 2125-2134.

Neiswanger, W. C., W., & Xing, E. (2013). Asymptotically exact, embarrassingly parallel mcmc. *arXiv preprint arXiv:1311.4780*.

Nichols, J. M., Link, W. A., Murphy, K. D., & Olson, C. C. (2010). A bayesian approach to identifying structural nonlinearity using free-decay response: Application to damage detection in composites. *Journal of Sound and Vibration*, *329*, 2995-3007.

Nichols, J. M., Moore, E. Z., & Murphy, K. D. (2011). Bayesian identification of a cracked plate using a population-based markov chain monte carlo method. *Computers and Structures*, *89*, 1323-1332.

Peng, T., Saxena, A., Goebel, K., Xiang, Y., & Liu, Y. (2014). Probabilistic damage diagnosis of composite laminates using bayesian inference. In *16th AIAA Non-Deterministic Approaches Conference.*

Peters, W. H., & Ranson, W. F. (1982). Digital imaging techniques in experimental stress analysis. *Optical Engineering*, *21*(3), 427-431.

Prudencio, E., Bauman, P. T., Faghihi, D., Ravi-Chandar, K., & Oden, J. T. (2015). A computational framework for dynamic data-driven material damage control, based on bayesian inference and model selection. *In-*

Error in Mean Estimate (%)				
	Sensor Array 1		Sensor Array 2	
	Known BC	Unknown BC	Known BC	Unknown BC
x	3.22	2.96	15.11	12.08
y	0.08	1.81	2.18	4.75
a	12.14	14.32	16.12	3.64
θ	11.30	10.05	64.13	46.10

Table 2. Mean estimate errors for crack characterization for known versus unknown boundary condition cases.

ternational Journal for Numerical Methods in Engineering, *102*(3-4), 379–403. Retrieved from http://dx.doi.org/10.1002/nme.4669 doi: 10.1002/nme.4669.

Prudencio, E., & Cheung, S. H. (2012). Parallel adaptive multilevel sampling algorithms for the bayesian analysis of mathematical models. *International Journal for Uncertainty Quantification*, *2*(3), 215–237.

Python Software Foundation. (2016). *Python language reference, version 2.7.* Retrieved from www.python.org

Sbarufatti, C., Manes, A., & Giglio, M. (2013). Performance optimization of a diagnostic system based upon a simulated strain field for fatigue damage characterization. *Mechanical Systems and Signal Processing*, *40*(2), 667 - 690. doi: http://dx.doi.org/10.1016/j.ymssp.2013.06.003.

Vrugt, J. A., ter Braak, C. F., Diks, C. H., Higdon, D., Robinson, B. A., & Hyman, J. M. (2009). Accelerating markov chain monte carlo simulation by differential evolution with self-adaptive randomized subspace sampling. *International Journal of Nonlinear Science and Numerical Simulation*, *10*(3), 273-290.

Wang, L., & Yuan, F. G. (2007). Active damage localization technique based on energy propagation of lamb waves. *Smart Structures and Systems*, *3*, 201-217.

Warner, J. E., Bomarito, G. B., Heber, G., & Hochhalter, J. D. (2016). Scalable implementation of finite elements by NASA - implicit (ScIFEi). NASA/TM-2016-219180.

Warner, J. E., & Hochhalter, J. D. (2016). Probabilistic damage characterization using a computationally-efficient bayesian approach. NASA/TP-2016-219169.

Yan, G. (2012). A bayesian approach for identification of structural crack using strain measurements. In *Sixth European Workshop on Structural Health Monitoring.* Dresden, Germany.